Numerical Investigations of Turbulent Flow Past a Generic Airship

Kamal El Omari, Éric Schall, Bruno Koobus, Alain Dervieux

INRIA

Numerical Investigations of Turbulent Flow Past a Generic Airship

Kamal El Omari — Eric Schall — Bruno Koobus — Alain Dervieux

N° 5455

Janvier 2005

Thème NUM

Rapport de recherche

Numerical Investigations of Turbulent Flow Past a Generic Airship

Kamal El Omari*, Eric Schall* , Bruno Koobus† , Alain Dervieux‡

Abstract: Turbulent separated flows around an airship-like geometry (a prolate spheroid 6:1) are investigated using three turbulence modelings based on statistical and Large Eddy Simulation (LES) approaches. The turbulence models used in the simulations are a standard high Reynolds k–ε model, a Smagorinsky LES model and a variational multiscale LES one. The flow of interest is characterized by a relatively low Mach number ($Mach = 0.15$), an angle of attack set to $20°$ and a Reynolds number fixed to 4×10^4. The three-dimensional compressible Navier-Stokes equations equipped with the previous turbulent models are discretized by a mixed finite element/finite volume method. The simulations show that the primary longitudinal vortex is predicted by the three models, but only the VMS-LES model predicts a secondary vortical flow structure that is observed in experimental studies.

Key-words: Turbulence, Reynolds Averaged Navier-Stokes, Large Eddy Simulation, Variational Multiscale, Prolate Spheroid, Finite Volume, Unstructured Grid

* LaTEP, IUT GTE, UPPA, 1 Av. de l'Université, 64000 Pau, FRANCE
† Université de Montpellier II, Dépt. Math., CC 051, F-34095 Montpellier Cedex 5, FRANCE
‡ INRIA, 2003 Route des Lucioles, F-06902 Sophia-Antipolis Cedex, FRANCE

Modélisations Numériques de l'Écoulement Turbulent Autour d'un Dirigeable Générique

Résumé : Les écoulements turbulents décollés autour d'une géométrie générique de dirigeable (ellipsoïde allongé 6 : 1) sont étudiés ici à l'aide de trois modèles de turbulence basés soit sur une approche statistique soit sur des simulations des grandes échelles (LES). Les modèles utilisés sont : le modèle standard haut Reynolds k–ε, le modèle LES Smagorinsky et un modèle LES variationnel multi-échelles (VMS-LES). L'écoulement étudié est caractérisé par un nombre de Mach relativement bas ($Mach = 0,15$), une incidence de 20° et un nombre de Reynolds de 4×10^4. Les équations tridimensionnelles et compressibles de Navier-Stokes, munies des modèles précédents, sont discrétisées par une méthode mixte éléments finis/volumes finis. Les simulations montrent que les trois modèles sont capables de prévoir le vortex longitudinal primaire, mais, que seul le modèle original VMS-LES a été en mesure de capturer numériquement le vortex secondaire observé dans le cadre d'études expérimentales de la littérature.

Mots-clés : Turbulence, modèle statistique RANS, simulation des grandes échelles, simulation variationnelle multi-échelles, ellipsoïde allongé, volumes finis, maillage non structuré

Contents

1   Introduction

In the context of an airship development program, we consider the numerical study of the flow around a flying generic airship. We are specially interested in flows involving rather large angle of attack around three-dimensional smooth bodies and in the phenomena induced by such flows, like separation-induced turbulent vortices. Problems involving flow separation in three-dimensional configurations is a very challenging topic in fluid dynamics research.

The investigated geometry is a prolate spheroid. It represents the closest shape to an airship geometry that can be found in the literature [1, 2]. Detached flows around prolate spheroids were the subject of several numerical studies [3, 4, 5, 6], principally in the aim of CFD codes assessments, specially when the flow separation is not induced by a geometrical feature as it is the case of submarine vehicles, aircrafts fuselages and ogives.

Most of the previously cited studies concerned by turbulent flows aroud prolate spheroids, and specially experimental ones [1, 2], have considered high Reynols number flows ($Re > 10^6$). A numerical study in these conditions demands the usage of very fine meshes and large CPU resources. In the scope of this first study we consider a less important Reynolds number $Re = 4 \times 10^4$ to be able to rapidly compare the results given by three different turbulence models: RANS $k - \varepsilon$, LES (Smagorinsky) and VMS-LES.

The Reynolds Averaged Navier-Stokes (RANS) two-equations statistical models are designed for providing steady mean flow fields. They generally rely on a Boussinesq turbulent viscosity. But this viscosity may be too large and may damp important steady and unsteady vortical flow structures. Non-equilibrium flows, as those arising close to leading edge at high angle of attack, are generally not accurately modeled. Our study starts with a set of results obtained with a standard two-equations model ($k - \varepsilon$) [7] combined with the Reichardt wall law [8].

In contrast to statistical models, Large Eddy Simulation (LES) ones are designed to the numerical simulation of the smallest details with respect to the grid size. Two LES models are applied to the calculation of this low-Reynolds flow: a Smagorinsky model which has been already applied with the same numerics in previous studies [9], and a Variational MultiScale (VMS) model [10, 11] which has the advantage to bring modeling only to the finest resolvable scales.

2 Turbulence modelings

2.1 The $k - \varepsilon$ two-equations turbulence model

The compressible Reynolds averaged Navier-Stokes (RANS) equations are expressed as follows (in a two-dimensional form for sake of briefness, the three-dimensional expression is straightforward):

$$\frac{\partial \mathbf{W}}{\partial t} + \nabla.\mathcal{F}(\mathbf{W}) = \nabla.\mathcal{R}(\mathbf{W}) \quad \text{where} \quad \mathbf{W} = (\rho, \rho v_1, \rho v_2, E)^T \qquad (1)$$

where W is the mean fluid state vector, $\mathcal{F}$ and $\mathcal{R}$ are respectively the convective and diffusive fluxes given by

$$\mathcal{F}(\mathbf{W}) = \begin{pmatrix} \mathcal{F}_1(\mathbf{W}) \\ \mathcal{F}_2(\mathbf{W}) \end{pmatrix} , \ \mathcal{R}(\mathbf{W}) = \begin{pmatrix} \mathcal{R}_1(\mathbf{W}) \\ \mathcal{R}_2(\mathbf{W}) \end{pmatrix} ,$$

in which

$$\mathcal{F}_1(\mathbf{W}) = \begin{pmatrix} \rho v_1 \\ \rho v_1^2 + p \\ \rho v_1 v_2 \\ (E + p) v_1 \end{pmatrix} , \ \mathcal{F}_2(\mathbf{W}) = \begin{pmatrix} \rho v_2 \\ \rho v_1 v_2 \\ \rho v_2^2 + p \\ (E + p) v_2 \end{pmatrix} ,$$

$$\mathcal{R}_1(\mathbf{W}) = \frac{\mu}{Re} \begin{pmatrix} 0 \\ \sigma_{11} \\ \sigma_{12} \\ v_1\sigma_{11} + v_2\sigma_{12} + \\ \frac{\gamma}{Pr}\frac{\partial e}{\partial x_1} \end{pmatrix} + \frac{1}{R_t} \begin{pmatrix} 0 \\ \sigma_{11} - \frac{2}{3}\rho k R_t \\ \sigma_{12} \\ v_1\sigma_{11} + v_2\sigma_{12} - \frac{2}{3}\rho k v_1 R_t + \\ \frac{\gamma}{Pr_t}\frac{\partial e}{\partial x_1} \end{pmatrix} ,$$

$$\mathcal{R}_2(\mathbf{W}) = \frac{\mu}{Re} \begin{pmatrix} 0 \\ \sigma_{12} \\ \sigma_{22} \\ v_1\sigma_{12} + v_2\sigma_{22} + \\ \dfrac{\gamma}{Pr}\dfrac{\partial e}{\partial x_2} \end{pmatrix} + \frac{1}{R_t} \begin{pmatrix} 0 \\ \sigma_{12} \\ \sigma_{22} - \frac{2}{3}\rho k R_t \\ v_1\sigma_{12} + v_2\sigma_{22} - \dfrac{2}{3}\rho k v_2 R_t + \\ \dfrac{\gamma}{Pr_t}\dfrac{\partial e}{\partial x_2} \end{pmatrix} ,$$

with:

$$E = \rho e + \tfrac{1}{2}\rho\|v\|^2 + \rho k \qquad , \qquad v = (v_1, v_2)^T \quad ,$$

$$p = (\gamma - 1)\rho e \qquad\qquad , \qquad \sigma = \nabla v + \nabla^T v - \frac{2}{3}\nabla.v I_d \quad ,$$

$$\gamma = \frac{c_p}{c_v}.$$

The closure of system (1) is achieved here by a two-equation high Reynolds $k - \varepsilon$ model governed by the following equations

$$\frac{\partial W_t}{\partial t} + \nabla.\mathcal{F}_t(\mathbf{W}_t) = \nabla.\mathcal{R}_t(\mathbf{W}_t) + \Omega(\mathbf{W}_t) ,$$

with

$$\mathbf{W}_t = \begin{pmatrix} \rho k \\ \rho \varepsilon \end{pmatrix}$$

where, for a two-dimensional flows, the fluxes $\mathcal{F}_t(\mathbf{W}_t)$ and $\mathcal{R}_t(\mathbf{W}_t)$ are given by

$$\mathcal{F}_t(\mathbf{W}_t) = \begin{pmatrix} \mathcal{F}_{t1}(\mathbf{W}_t) \\ \mathcal{F}_{t2}(\mathbf{W}_t) \end{pmatrix}, \mathcal{R}_t(\mathbf{W}_t) = \begin{pmatrix} \mathcal{R}_{t1}(\mathbf{W}_t) \\ \mathcal{R}_{t2}(\mathbf{W}_t) \end{pmatrix},$$

in which:

$$\mathcal{F}_{t1}(\mathbf{W}_t) = \begin{pmatrix} \rho v_1 k \\ \rho v_1 \varepsilon \end{pmatrix}, \mathcal{F}_{t2}(\mathbf{W}_t) = \begin{pmatrix} \rho v_2 k \\ \rho v_2 \varepsilon \end{pmatrix},$$

$$\mathcal{R}_{t1}(\mathbf{W}_t) = \begin{pmatrix} \left(\dfrac{\mu}{Re} + \dfrac{1}{\sigma_k R_t}\right) \dfrac{\partial k}{\partial x_1} \\ \left(\dfrac{\mu}{Re} + \dfrac{1}{\sigma_\varepsilon R_t}\right) \dfrac{\partial \varepsilon}{\partial x_1} \end{pmatrix} \; , \; \mathcal{R}_{t2}(\mathbf{W}_t) = \begin{pmatrix} \left(\dfrac{\mu}{Re} + \dfrac{1}{\sigma_k R_t}\right) \dfrac{\partial k}{\partial x_2} \\ \left(\dfrac{\mu}{Re} + \dfrac{1}{\sigma_\varepsilon R_t}\right) \dfrac{\partial \varepsilon}{\partial x_2} \end{pmatrix}$$

and

$$\Omega(\mathbf{W}_t) = \begin{pmatrix} -\rho\varepsilon + \mathcal{P} \\ -c_{\varepsilon 2}\dfrac{\rho\varepsilon^2}{k} + c_{\varepsilon 1}\dfrac{\varepsilon}{k}\mathcal{P} \end{pmatrix} \; ,$$

$$\mathcal{P} = -\frac{2}{3}\rho k \nabla.v + \frac{1}{R_t}\left[-\frac{2}{3}(\nabla.v)^2 + \sum_{i,j=1,2}\left[\left(\frac{\partial v_i}{\partial x_j}\right)^2 + \frac{\partial v_i}{\partial x_j}\frac{\partial v_j}{\partial x_i} \right] \right];$$

$\mathcal{P}$ is the turbulent energy production. The turbulent Reynolds number R_t is obtained from the eddy viscosity μ_t:

$$\frac{1}{R_t} = \mu_t = c_\mu\frac{\rho k^2}{\varepsilon},$$

and the closure coefficients σ_k, σ_ε, $c_{\varepsilon 1}$, $c_{\varepsilon 2}$ and c_μ are set to their standard values:

$$\sigma_k = 1.0 \; ; \; \; \sigma_\varepsilon = 1.3 \; ; \; \; c_{\varepsilon 1} = 1.44 \; ; \; \; c_{\varepsilon 2} = 1.92 \; ; \; \; c_\mu = 0.09 \; .$$

2.2   Large Eddy Simulation with Smagorinsky model

LES models are based on a spatial filtering of the Navier-stokes equations with respect to a filter width Δ. Only the large scales corresponding to the filtered flow variables are directly simulated, and modeling is introduced to take into account the effect of the unresolved subgrid scales on these large scales. In this study, the well known Smagorinsky model is used.

The filtered field of a quantity f in a given space domain $\mathcal{D}$ is obtained by convolution with a filter function $G_\Delta(\mathbf{x})$ and is defined by

$$\overline{f}(\mathbf{x}, t) = \int_{\mathcal{D}} f(\mathbf{y}, t) G_\Delta(\mathbf{x} - \mathbf{y}) d\mathbf{y} \tag{2}$$

This quantity can then be written as $f = \overline{f} + f'$ where f' is the fluctuations of this function at scales smaller than the filter width Δ.

In addition, for compressible flows, a density-weighted filter (Favre filter) is introduced as $\tilde{f} = \dfrac{\overline{\rho f}}{\overline{\rho}}$. The filtered Navier-Stokes equations become after the application of Smagorinsky modeling:

$$\frac{\partial \overline{\rho}}{\partial t} + \frac{\partial \overline{\rho} \tilde{u}_i}{\partial x_j} = 0 \tag{3}$$

$$\frac{\partial (\overline{\rho} \tilde{u}_i)}{\partial t} + \frac{\partial (\overline{\rho} \tilde{u}_i \tilde{u}_j)}{\partial x_j} = -\frac{\partial \Pi}{\partial x_j} + \frac{\partial \left[(\mu + \mu_t) \left(2\tilde{S}_{ij} - \frac{2}{3}\tilde{S}_{ii}\delta_{ij} \right) \right]}{\partial x_j} \tag{4}$$

$$\frac{\partial (\overline{\rho} \tilde{e})}{\partial t} + \frac{\partial \left[(\overline{\rho} \tilde{e} + \Pi) \tilde{u}_j \right]}{\partial x_j} = \frac{\partial \left[\tilde{u}_j \mu \left(2\tilde{S}_{ij} - \frac{2}{3}\tilde{S}_{ii}\delta_{ij} \right) \right]}{\partial x_j} \tag{5}$$

$$+ \frac{\partial}{\partial x_j} \left[\left(\frac{C_p \mu_t}{Pr_t} + K \right) \frac{\partial \Theta}{\partial x_j} \right] \tag{6}$$

and the constitutive equations are

$$\Pi = \overline{\rho} R \Theta \quad , \quad \tilde{e} = C_v \Theta + \frac{1}{2}(\|\tilde{u}\|^2) \quad , \quad S_{ij} = \frac{1}{2}\left(\frac{\partial \mathbf{u}_i}{\partial \mathbf{x}_j} + \frac{\partial \mathbf{u}_j}{\partial \mathbf{x}_i} \right) \quad ,$$

$$\mu_t = \overline{\rho}(C_s \Delta)^2 \sqrt{2\tilde{S}_{ij}\tilde{S}_{ij}}, \tag{7}$$

where μ_t is the eddy viscosity introduced by the Smagorinsky model (Eq. 7). The complete definition of μ_t needs the definition of the filter width Δ and the Smagorinsky constant C_s. This constant is set to 0.18 and the filter width associated to a tetrahedron T_j is defined by

$$\Delta_j = \sqrt[3]{Vol(T_j)}. \tag{8}$$

The details of the derivation of the previous equations can be found in [12].

2.3   The Variational Multiscale modeling of turbulence

Unlike the classical LES approach, the variational multiscale LES (VMS-LES) model is not based on a spatial filtering of the Navier-Stokes equations but on a variational projection of these equations on a coarse-scales space and a fine-scales space [10]. The VMS-LES method separates the scales *a priori*, that is before the simulation is started. Furthermore, the VMS-LES method models the effects of the unresolved scales only in the equations governing the finest resolved scales and not on the equations governing the whole resolved scales as the LES method does.

Let Ω be the flow domain discretized by a tetrahedral mesh, from which a dual finite-volume mesh is derived [14]. Convective fluxes are treated here by a finite volume method in which a variable w is approximated first by a constant in each control volume as $w = \sum_i w_i \mathcal{X}_i$, where $\mathcal{X}_i$ is the characteristic function corresponding to the control volume C_i associated with node i, and w_i denotes the constant value of w in this control volume. Next, this first-order approximation is transformed into a higher-order spatial discretization by a MUSCL approach [13]. The diffusive fluxes are treated by a finite-element method in which a flow variable w is approximated by a continuous piecewise linear function. This can be written as $w = \sum_i w_i \Phi_i$, where Φ_i is the P1 shape function associated with node i, and w_i denotes the value of w at this node.

The semi-discretization of the compressible Navier-Stokes equations by the mixed element volume method with mass lumping leads to the following system of equations

$$
\begin{cases}
A(\mathcal{X}_i, \mathbf{W}) \quad = \int_\Omega \frac{\partial \rho}{\partial t} \mathcal{X}_i \, d\Omega \; + \; \int_{\partial Sup\mathcal{X}_i} \rho \mathbf{u.n}\mathcal{X}_i \, d\Gamma = 0 \\[2ex]
\mathbf{B}(\mathcal{X}_i, \Phi_i, \mathbf{W}) \; = \int_\Omega \frac{\partial \rho \mathbf{u}}{\partial t} \mathcal{X}_i \, d\Omega \; + \; \int_{\partial Sup\mathcal{X}_i} \rho \, \mathbf{u} \otimes \mathbf{u} \, \mathbf{n}\mathcal{X}_i \, d\Gamma \\[2ex]
\qquad\qquad\qquad\quad + \int_{\partial Sup\mathcal{X}_i} P\mathbf{n}\mathcal{X}_i \, d\Gamma \; + \; \int_\Omega \sigma \nabla \Phi_i \, d\Omega = \mathbf{0} \\[2ex]
C(\mathcal{X}_i, \Phi_i, \mathbf{W}) \; = \int_\Omega \frac{\partial E}{\partial t} \mathcal{X}_i \, d\Omega \; + \; \int_{\partial Sup\mathcal{X}_i} (E + P)\mathbf{u.n}\mathcal{X}_i \, d\Gamma \\[2ex]
\qquad\qquad\qquad\quad + \int_\Omega \sigma \mathbf{u}.\nabla \Phi_i \, d\Omega \; + \; \int_\Omega \lambda \nabla T.\nabla \Phi_i \, d\Omega = 0
\end{cases}
\tag{9}
$$

where $\mathbf{W} = (\rho, \mathbf{u}, T)^T$ and $\partial Sup\mathcal{X}_i$ denotes the boundary of the support of $\mathcal{X}_i$, and $\mathbf{n}$ is the outward normal to this support.

Let $\mathcal{V}_{FV}$ and $\mathcal{V}_{FE}$ denote respectively the space spanned by the the characteristic functions $\{\mathcal{X}_k\}$, and that spanned by the P1 shape functions $\{\Phi_k\}$. In order to separate *a priori* the coarse and fine scales, these spaces are decomposed as follows

$$\mathcal{V}_{FV} = \overline{\mathcal{V}}_{FV} \oplus \mathcal{V}'_{FV} \quad , \quad \mathcal{V}_{FE} = \overline{\mathcal{V}}_{FE} \oplus \mathcal{V}'_{FE}. \tag{10}$$

Here the overline refers to the coarse scales, and the $'$ superscript to the fine scales. Hence, consistently with Eqs. (10), $\mathbf{W}$ is decomposed into a coarse scale component $\overline{\mathbf{W}}$ and a fine scale part $\mathbf{W}'$ as $\mathbf{W} = \overline{\mathbf{W}} + \mathbf{W}'$. This decomposition relies on coarse finite-volume cells which are built by agglomeration of a small number of fine dual control volumes.
From this decomposition, the problem (9) is transformed into the two following subproblems

$$\begin{cases} A(\overline{\mathcal{X}}_i, \overline{\mathbf{W}} + \mathbf{W}') & = 0 \\ \mathbf{B}(\overline{\mathcal{X}}_i, \overline{\Phi}_i, \overline{\mathbf{W}} + \mathbf{W}') & = \mathbf{0} \\ C(\overline{\mathcal{X}}_i, \overline{\Phi}_i, \overline{\mathbf{W}} + \mathbf{W}') & = 0 \end{cases} \quad \begin{cases} A(\mathcal{X}'_i, \overline{\mathbf{W}} + \mathbf{W}') & = 0 \\ \mathbf{B}(\mathcal{X}'_i, \Phi'_i, \overline{\mathbf{W}} + \mathbf{W}') & = \mathbf{0} \\ C(\mathcal{X}'_i, \Phi'_i, \overline{\mathbf{W}} + \mathbf{W}') & = 0 \end{cases} \tag{11}$$

Without giving the details of the model derivation – that the reader can find in [11] –, we can say that this decomposition gives two sets of equations, one governing the coarse resolved scales and the other one the fine resolved scales. These sets of equations are coupled. Some terms that appear in the fine resolved scales equations require some modeling (unless all scales are resolved by means of DNS). This

is achieved through a compressible generalized Smagorinsky eddy viscosity model involving only the fine resolved scales. Then, the final form of these equations writes

$$
\begin{cases}
\displaystyle\int_\Omega \frac{\partial \rho}{\partial t}\mathcal{X}_i \, d\Omega \; + \; \int_{\partial Sup\mathcal{X}_i} \rho\mathbf{u.n}\mathcal{X}_i \, d\Gamma & = 0 \\[2ex]
\displaystyle\int_\Omega \frac{\partial \rho\mathbf{u}}{\partial t}\mathcal{X}_i \, d\Omega \; + \; \int_{\partial Sup\mathcal{X}_i} \rho\,\mathbf{u}\otimes\mathbf{u}\,\mathbf{n}\mathcal{X}_i \, d\Gamma \; + \; \int_{\partial Sup\mathcal{X}_i} P\mathbf{n}\mathcal{X}_i \, d\Gamma & \\[1ex]
\displaystyle + \int_\Omega \sigma\nabla\Phi_i \, d\Omega \; + \; \int_\Omega \tau'\nabla\Phi'_i \, d\Omega & = \mathbf{0} \qquad (12) \\[2ex]
\displaystyle\int_\Omega \frac{\partial E}{\partial t}\mathcal{X}_i \, d\Omega \; + \; \int_{\partial Sup\mathcal{X}_i} (E+P)\mathbf{u.n}\mathcal{X}_i \, d\Gamma \; + \; \int_\Omega \sigma\mathbf{u}.\nabla\Phi_i \, d\Omega & \\[1ex]
\displaystyle + \int_\Omega \lambda\nabla T.\nabla\Phi_i \, d\Omega \; + \; \int_\Omega \frac{C_p\mu'_t}{Pr_t}\nabla T'.\nabla\Phi'_i \, d\Omega & = 0
\end{cases}
$$

where

$$
\tau'_{ij} \;=\; \mu'_t(2S'_{ij} - \frac{2}{3}S'_{kk}\delta_{ij}) \tag{13}
$$

$$
S'_{ij} \;=\; \frac{1}{2}(\frac{\partial \mathbf{u}'_i}{\partial \mathbf{x}_j} + \frac{\partial \mathbf{u}'_j}{\partial \mathbf{x}_i}) \tag{14}
$$

$$
\mu'_t \;=\; \overline{\rho}(C'_s\Delta')^2|S'| \tag{15}
$$

$$
|S'| \;=\; \sqrt{2S'_{ij}S'_{ij}}, \tag{16}
$$

$C'_s = 0.1$ and Δ' denotes the local grid size. In this work, Δ' has the same definition as in Eq. (8).

2.4   Wall law

In all the simulations presented in this study, the flow domain is extended only up to a wall boundary located at a distance δ from the surface of the prolate. In the

evaluation of the viscous fluxes, the wall shear stress is computed as $\tau_w = \rho u_f^2$ where the friction velocity u_f is determined from the non-linear Reichardt's law

$$U_{|\delta}^+ = 2.5 \log(1 + 0.41\delta^+) + 7.8 \left(1 - e^{-\delta^+/11} - \frac{\delta^+}{11} e^{-0.33\delta^+} \right) \tag{17}$$

in which

$$\delta^+ = \frac{u_f}{\nu}\delta \quad \text{and} \quad U_{|\delta}^+ = \frac{(v.n^\perp)_{|\delta}}{u_f}.$$

3 Numerical issues

In this work, the spatial discretization of the Navier-Stokes equation is achieved on unstructured tetrahedral meshes by a mixed element/volume formulation [16, 8], where the convective terms are discretized by a finite volume method and the diffusive terms are approximated by a Galerkin method using P_1 shape functions. The scheme described below applies for the three turbulence models, provided that the equations are written in the generic form of Eq. (1).

3.1 Convective fluxes

The convective fluxes are approached by the Roe's scheme [15] which is used together with a MUSCL linear reconstruction method [13, 14] to obtain a higher order of spatial accuracy (second-order was used in the scope of this paper).

Let $V(i)$ be the set of neighboring nodes to a vertex i. The convective fluxes through the dual cell boundaries surrounding the vertex i wrote:

$$\int_{\partial C_i} \mathcal{F}(\mathbf{W}).\mathbf{n} \; d\Gamma = \sum_{j \in V(i)} \int_{\partial C_i \cap \partial C_j} \mathcal{F}(\mathbf{W}).\mathbf{n} \; d\Gamma \tag{18}$$

where the boundary $\partial C_i \cap \partial C_j$ is located between the two cells centered at nodes i and j. The fluxes of Eq. (18) are approximated by the numerical fluxes

$$\sum_{j \in V(i)} \Phi(\mathbf{W}_{ij}, \mathbf{W}_{ji}, \mathbf{n}_{ij}) \quad \text{with} \quad \mathbf{n}_{ij} = \int_{\partial C_i \cap \partial C_j} \mathbf{n} \; d\Gamma$$

and, following the Roe's scheme:

$$\Phi(\mathbf{W}_{ij}, \mathbf{W}_{ji}, \mathbf{n}_{ij}) = \frac{\mathcal{F}(\mathbf{W}_{ij}, \mathbf{n}_{ij}) + \mathcal{F}(\mathbf{W}_{ji}, \mathbf{n}_{ij})}{2} - \gamma_s \, \mathbf{d}(\mathbf{W}_{ij}, \mathbf{W}_{ji}, \mathbf{n}_{ij}). \qquad (19)$$

The upwind term is given by

$$\mathbf{d}(\mathbf{W}_{ij}, \mathbf{W}_{ji}, \mathbf{n}_{ij}) = |R(\mathbf{W}_{ij}, \mathbf{W}_{ji}, \mathbf{n}_{ij})| \frac{\mathbf{W}_{ji} - \mathbf{W}_{ij}}{2} \; . \qquad (20)$$

where R is the Roe Matrix:

$$R(\mathbf{W}_{ij}, \mathbf{W}_{ji}, \mathbf{n}_{ij}) = \frac{\partial \mathcal{F}}{\partial \mathbf{W}} \left(\widehat{\mathbf{W}}, \mathbf{n}_{ij} \right) \qquad (21)$$

$\widehat{\mathbf{W}}$ is the Roe average of the vector $\mathbf{W}$. The amount of numerical viscosity introduced by the the upwind term is controlled by the multiplicative coefficient γ_s.

The state vectors $\mathbf{W}_{ij}$ and $\mathbf{W}_{ji}$ are reconstructed values of $\mathbf{W}$ at the boundary $\partial C_i \cap \partial C_j$ as

$$\mathbf{W}_{ij} = \mathbf{W}_i + \frac{1}{2}(\nabla \mathbf{W})_{ij}.\mathbf{ij}$$
$$\mathbf{W}_{ji} = \mathbf{W}_j - \frac{1}{2}(\nabla \mathbf{W})_{ji}.\mathbf{ij}.$$

The gradients $(\nabla \mathbf{W})_{ij}$ and $(\nabla \mathbf{W})_{ji}$ are computed by a β-scheme which blends centered and upwind gradients:

$$\begin{array}{ll} (\nabla \mathbf{W})_{ij}.\mathbf{ij} = & (1 - 2\beta)(\nabla \mathbf{W})^C_{ij}.\mathbf{ij} + 2\beta(\nabla \mathbf{W})^U_i.\mathbf{ij} \\ (\nabla \mathbf{W})_{ji}.\mathbf{ij} = & (1 - 2\beta)(\nabla \mathbf{W})^C_{ji}.\mathbf{ij} + 2\beta(\nabla \mathbf{W})^U_j.\mathbf{ij} \end{array} \qquad (22)$$

where

$(\nabla \mathbf{W})^C_{ij}.\mathbf{ij} = \mathbf{W}_j - \mathbf{W}_i$: centered gradient
$(\nabla \mathbf{W})^U_i$: volumetric average of the $P1$-Galerkin gradients of the tetrahedra surrounding the vertex i. β is taken equal to $\frac{1}{3}$.

Because of the low Mach number value of the studied flow, no flux limitation was used here.

3.2   Diffusive fluxes

Diffusive fluxes are approximated by a Galerkin method using $P1$ shape functions φ_i so

$$\sum_{\mathcal{T}(t),\, i \in \mathcal{T}(t)} \int_{\mathcal{T}(t)} \mathcal{R}(W).\nabla\varphi_i \, dD_x = \sum_{\mathcal{T}(t),\, i \in \mathcal{T}(t)} \text{Area}(\mathcal{T})\mathcal{R}(\mathcal{T}).\nabla\varphi_{i|_{\mathcal{T}}} \qquad (23)$$

$\mathcal{R}(\mathcal{T})$ denotes the constant value of $\mathcal{R}$ on the tetrahedron $\mathcal{T}$. The effect of the diffusive fluxes on the far-field is neglected.

Temporal scheme is implicit, second-order accurate and the computer code is parallelized using a non-overlapping domain decomposition. More details on the numerical approach of the used code (AERO3D) can be found in [8, 12, 9, 11].

4   Description of the test-case

We are interested in a flow around a 6:1 prolate spheroid of length $L = 1.37\,m$, at 20° angle of attack. The flow has the following far-field characteristics

- Mach number $M_\infty = 0.15$;

- Reynolds number $Re = \dfrac{V_\infty L}{\nu} = 4 \times 10^4$;

- density $\rho_\infty = 1.1\ kg\,m^{-3}$;

- pressure $p_\infty = 101300\ Pa$.

- The laminar-turbulent transition is fixed at $x/L = 0.2$.

The three-dimensional unstructured mesh used in the simulations is displayed in Fig. 1. It contains approximately 160000 nodes and 950000 tetrahedra. The computational domain dimensions are $7.2\,m \times 4.8\,m \times 4.8\,m$. These dimensions were judged sufficient by other authors of previous numerical studies [3]. The part of the mesh that is adjacent to the prolate surface is pseudo-structured, so that the heights of the first elements from this surface were fixed below $7 \times 10^{-3}m$. These values result in y^+ values that lie between 4 and 23. The numerical viscosity coefficient γ_s (Eq. 19) is set to 0.1 in the scope of this work.
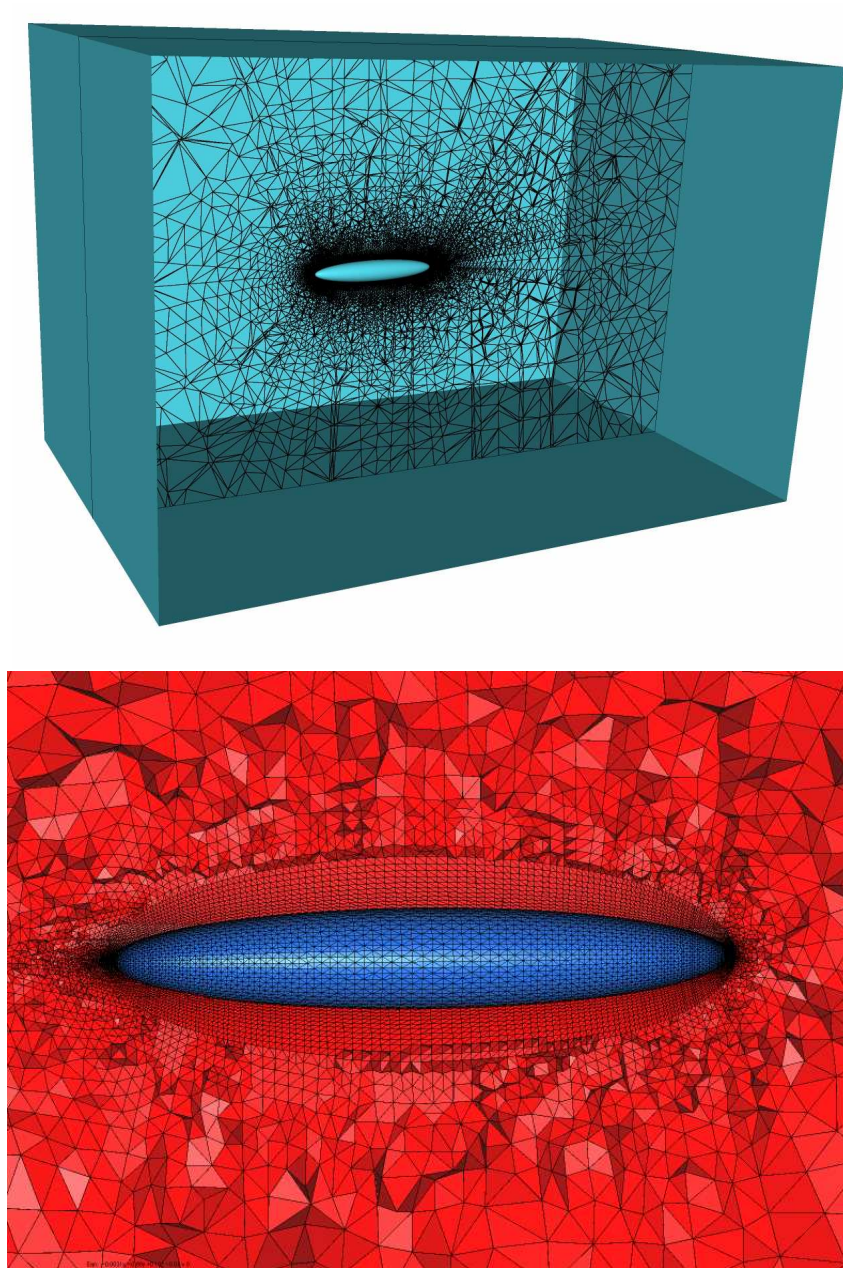
Figure 1: View of the whole domain with a mesh cut in the vertical symmetry plane (top) and zoom of the prolate (bottom)
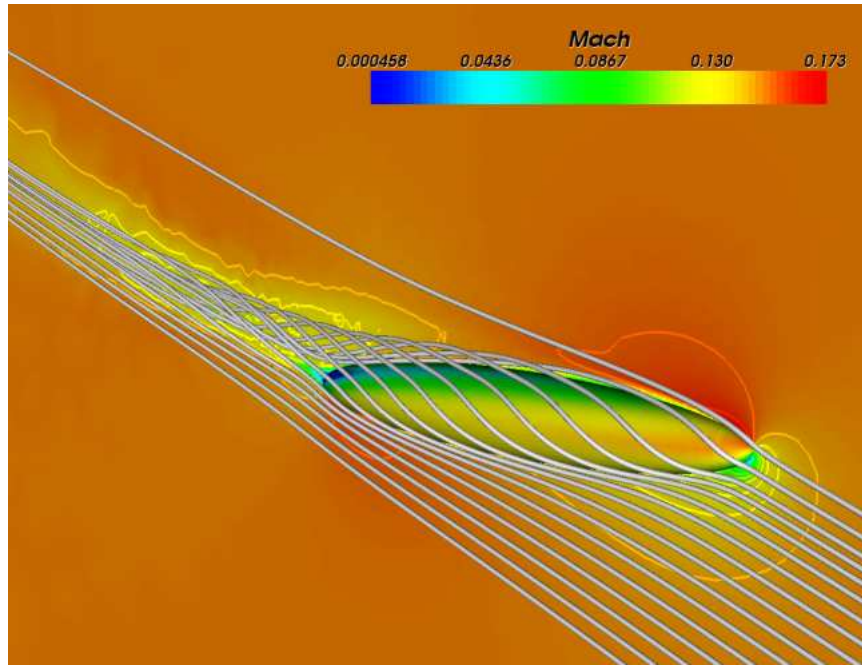
5 Results

Figure 2: Trajectories and Mach number around the prolate (VMS-LES model)

Three runs were performed corresponding to the three turbulence models presented in this paper. We give first, in Fig. 2, an idea of the fluid trajectories encountered in such a flow as well as the Mach number distribution obtained by the VMS-LES model. We compare the three models afterwards.

Fig. 3 displays the isovalues of the streamwise velocity obtained with these models in cross-planes located on the rear part of the prolate. We can notice that the vortices predicted by LES and VMS-LES models are better captured, and that the VMS-LES calculation shows more flow details than the LES and RANS models. Indeed, these two last models tend to introduce a too large amount of turbulent viscosity which damps the turbulent structures.

Fig. 4 depicts the fluid velocity vectors and streamlines in the cross-plane located at $x = 1.2\,m$. It confirms the previous observations, and we also notice that the VMS-LES model is able to capture a secondary vortex that is not predicted by the two
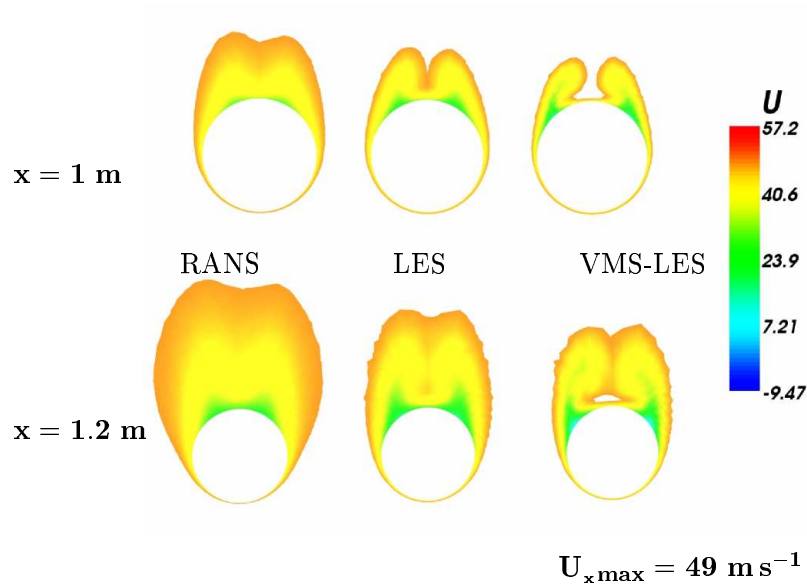
$$\mathbf{U_{x\,max} = 49\ m\,s^{-1}}$$

Figure 3: Streamwise velocity isovalues on cross-planes at $x = 1\ m$ and $x = 1.2\ m$

others models. Such a vortical flow structure is effectively observed by experimental and numerical studies with higher Reynolds number [2, 3].

We have seen that the three models exhibit perceptible differences concerning the longitudinal vortices, but the comparison of the behavior of pressure at the prolate surface shows that this quantity remains almost the same, specially on the symmetry line as shown in Fig. 5. At the $x = 1.2\,m$ position of the prolate surface, the examination of this quantity shows again that the VMS-LES exhibits some features not observed by the two other models like the negative pressure coefficient on the leeward.

Aerodynamic lift (C_l) and drag (C_d) coefficients relative to pressure and viscous forces are given in Tab. 1. They are respectively based on the reference surfaces $S_x = \pi(L/12)^2$ and $S_y = \pi L^2/24$. This table values show that the calculated drag is the lower when the turbulence model introduces less amount of numerical viscosity as it is the case of the VMS-LES model.
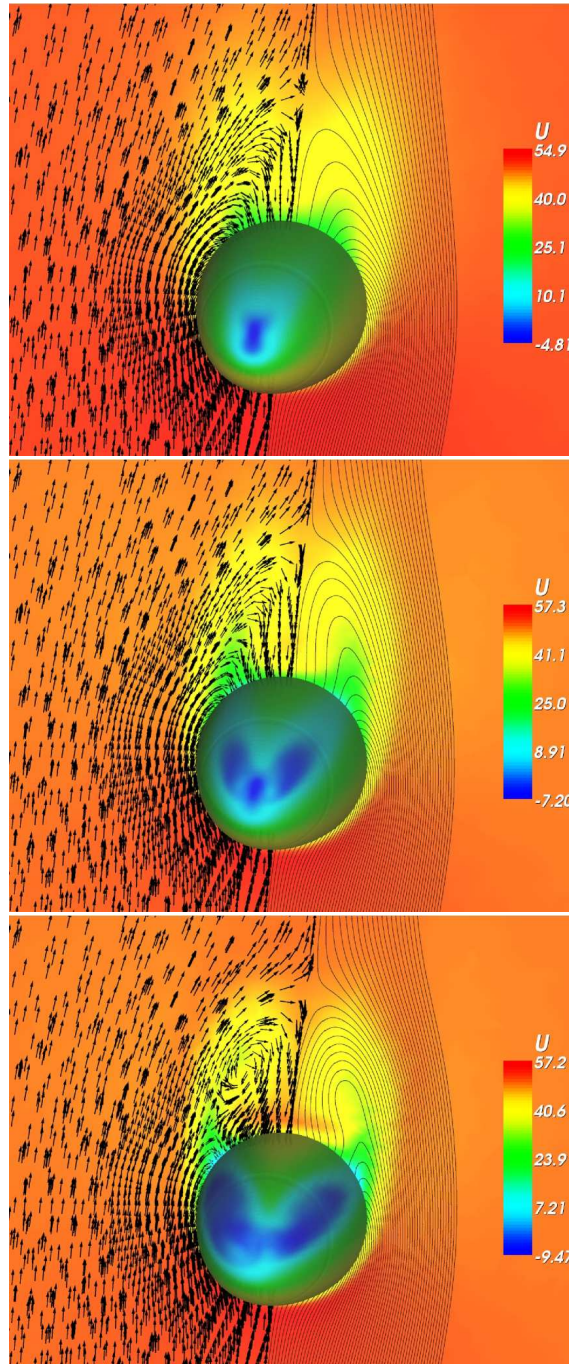
Figure 4: Velocity vectors and streamlines on cross-plane at $x = 1.2\,m$: RANS (top), LES (center), VMS-LES(bottom)
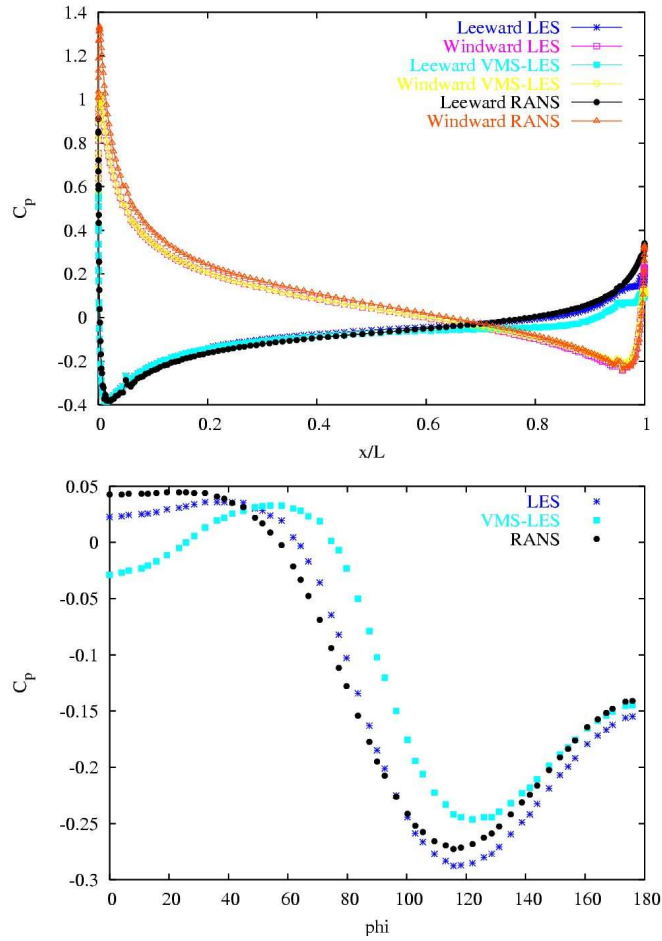
Figure 5: Pressure Coefficient C_p on the prolate surface at $z = 0$ (top) and at $x = 1.2\,m$ (bottom)

	C_d	C_l
RANS	0.194520	0.022696
LES	0.142107	0.009292
VMS-LES	0.139822	0.026346

Table 1: Aerodynamic coefficients of the prolate at 20° angle of attack

6   Conclusion

We have investigated the simulation of a low Mach compressible flow around an airship-like geometry using three turbulent models based on statistical and LES approaches. With this geometry, the flow separation is due to adverse pressure gradients in the azimuthal direction and not to geometry singularities, in contrast to many vortex shedding simulations achieved with the VMS-LES model in previous works. The study shows that, for flows with high angle of attack and strong boundary layer separation, low viscosity models like the VMS-LES model, are more suitable for capturing the main vortical flow structures. With this low Reynolds case, the three models are not very CPU consuming and of about the same cost. But the use of LES based models may be prohibitive for high Reynolds number flow calculations. Then a good compromise would be a blend of VMS-LES and classical RANS models.

Acknowledgements

References

[1] H.P. KREPLIN. Three-dimensional boundary layer and flow field data of an inclined prolate spheroid. Test Case ID: GE-20, *AGARD FDP WG-14 Experimental test cases for CFD validation* (1995).

[2] C.J. CHESNAKAS AND R.L. SIMPSON. A Detailed Investigation of the 3-*D* Separation about a 6:1 Prolate Spheroid at Angle of Attack,*AIAA Journal, 35,* 6 (1997), 990-999.

[3] G.S. CONSTANTINESCU, H. PASINATO, Y.Q. WANG, J.R. FORSYTHE AND K.D. SQUIRES. Numerical Investigation on Flow Past a Prolate Spheroid. *J. Fluids Eng., 124* (2002), 904-910.

[4] S.H. RHEE AND T. HINO. Computational Investigation of 3D Turbulent Flow Separation around a Spheroid using an Unstructured Grid Method. *Journal of the Society of Naval Architects of Japan, 188* (2000).

[5] V. C. PATEL AND S. E. KIM. Topology of laminar flow on a spheroid at incidence. *Computers and Fluids, 23*, 7 (1994) 939-953.

[6] J. PIQUET AND P. QUEUTEY. Navier-Stokes computations past a prolate spheroid at incidence—I. Low incidence case. *Computers and Fluids, 21*, 4 (1992) 599-625.

[7] B.E. LAUNDER AND D.B. SPALDING. The numerical computation of turbulent flows. *Comput. Methods Appl. Mech. Engrg., 3* (1974) 269-289.

[8] B. KOOBUS, C. FARHAT. AND H. TRAN, Computation of unsteady viscous flows around moving bodies using the k–ε turbulent model on unstructured dynamic grids. *Comput. Methods Appl. Mech. Engrg., 190* (2000) 1441-1466.

[9] S. CAMARRI, M.V. SALVETTI, B. KOOBUS AND A. DERVIEUX. Large-eddy simulation of a bluff-body flow on unstructured grids. *Int. J. Numer. Methods Fluids, 40* (2002), 1431-1460.

[10] T.J.R. HUGHES, L. MAZZEI AND K.E. JANSEN. Large eddy simulation and the variational multiscale method, *Comp. Vis. Sci.*, 3, 47, 2000.

[11] B. KOOBUS AND C. FARHAT. A Variational Multiscale Method for the Large Eddy Simulation of Compressible Turbulent Flows on Unstructured Meshes - Application to Vortex Shedding. *Comput. Methods Appl. Mech. Eng., 193*, 15-16 (2004) 1367-1383. *(also published as INRIA research report, N° 4722, February 2003)*

[12] S. CAMARRI, M.V. SALVETTI, Towards the Large-Eddy simulation of complex engineering flows with unstructured grids. *INRIA research report, N° 3844, December 1999.*

[13] B. VAN LEER, Towards the ultimate conservative difference scheme V: a second-order sequel to Godunov's method, *J. Comp. Phys., 32* (1979), 361-370.

[14] A. DERVIEUX, Steady Euler Simulations Using Unstructured Meshes, *Von Karman Institute Lecture Series*, (1985).

[15] P.L. ROE, Approximate Riemann solver, parameters vectors and difference schemes, *J. Comp. Phys., 43* (1981), 357-371.

[16] S. CAMARRI, M.V. SALVETTI, A. DERVIEUX. AND B. KOOBUS A low diffusion MUSCL scheme for LES on unstructured grids. *INRIA research report, N⁰ 4512, July 2002.*